Origin of the OH Vibrational Blue Shift in the LiOH Crystal

Kersti Hermansson,* Grzegorz Gajewski, and Pavlin D. Mitev

Materials Chemistry, The Ångström Laboratory, Uppsala University, Box 538, S-75121 Uppsala, Sweden

Received: March 19, 2008; Revised Manuscript Received: August 03, 2008

The O−H vibrational frequency in crystalline hydroxides is either upshifted or downshifted by its crystalline surroundings. In the LiOH crystal, the experimental gas-to-solid O−H frequency upshift ("blue shift") is approximately +115 cm^{-1}. Here plane-wave DFT calculations for the isotope-isolated LiOH crystal have been performed and we discuss the origin of the OH frequency upshift, and the nature of the OH group and the interlayer interactions. We find that (1) the vibrational frequency upshift originates from interactions *within the LiOH layer*; this OH upshift is slightly lessened by the *interlayer* interactions; (2) the interlayer O−H - - - H−O interaction is largely electrostatic in character (but there is no hydrogen bonding); (3) the gas-to-solid vibrational shift for OH in LiOH(s) and its subsystems qualitatively adheres to a parabola-like "frequency vs electric field strength" correlation curve, which has a maximum for a positive electric field, akin to the correlation curve earlier found in the literature for an isolated OH^- ion in an electric field.

1. Introduction

The water OH stretching vibrational frequency in *crystalline hydrates* is typically found in the range 3100−3600 cm^{-1}. The experimentally measured symmetric and antisymmetric stretching frequencies for the gas-phase water molecule lie at 3657 and 3756 cm^{-1}, respectively.[1] The OH frequencies are thus always downshifted by the intermolecular interactions when the water molecule is bound in a crystal. In *crystalline hydroxides*, the OH frequencies are found in a similar range, typically 3400−3700 cm^{-1}, but because the vibrational frequency of the gas-phase OH^- ion lies at 3556 cm^{-1},[2] the OH^- frequency is *either upshifted* ("blue-shifted") *or downshifted* ("red-shifted") by the intermolecular interactions in the crystal. This phenomenon is quite unusual: i.e., that intermolecular interactions in a crystal can *strengthen* the intramolecular bonds, but it happens for the OH^- ion. The overall context of the present article is to shed light on the correlation between the structure and OH frequency in crystalline hydroxides. The specific focus here is the origin behind the large gas-to-crystal OH frequency upshift observed experimentally in LiOH, approximately +115 cm^{-1}.

The LiOH crystal is a good model system for an "upshifting hydroxide" because it has a layered structure, which is a typical feature for many simple hydroxides and minerals, and because its structure is well-known from X-ray and neutron diffraction investigations (e.g., refs 3−5). The structure consists of neutral LiOH layers with OH groups pointing toward each other across the interlayer region in an antiparallel staggered fashion (Figure 1). The measured fundamental frequencies of the Raman-active A_{1g}[6] and the IR-active A_{2u}[7,8] O−H stretching modes in LiOH lie close to 3670 cm^{-1} and the corresponding gas-to-solid frequency shifts thus lie close to +115 cm^{-1}, as mentioned.

We are aware of three previous periodic electronic structure calculations for the LiOH crystal, namely the local basis-set B3LYP calculations of Tanigawa and Tanaka,[9] and of Mérawa et al.,[10] and our own plane-wave DFT calculations (Gajewski et al.[11]). In both refs 9 and 10, the anharmonic OH vibrational frequency for the Raman-active mode was derived from 1-D mode-following vibrational calculations based on potential energy curves obtained from the electronic structure calculations. In ref 11 we claimed that such an anharmonic treatment is inadequate for LiOH, because it underestimates the anharmonic contribution to the A_{1g} mode by ∼40% and gives a large anharmonic contribution in the wrong direction for the A_{2u} mode. On the other hand, a vibrational model with coupled 2-D anharmonic oscillators was found to yield absolute frequencies

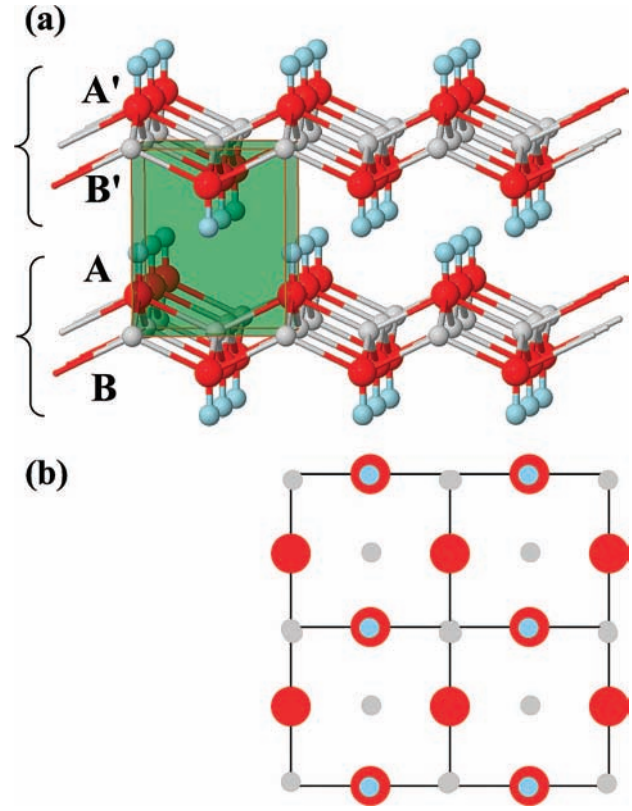

Figure 1. The structure of the lithium hydroxide crystal. Several crystallographic unit cells are shown, from the side in (a), and from above in (b). The space group is tetragonal (*P4/nmm*), there are two formula units per crystallographic cell, and the experimental cell parameters are $a = 3.549$ Å and $c = 4.334$ Å.[3−5] The *A, B, A′* and *B′* labels of different OH layers are referred to in the text.

10.1021/jp802426d CCC: $40.75
Published on Web 11/25/2008

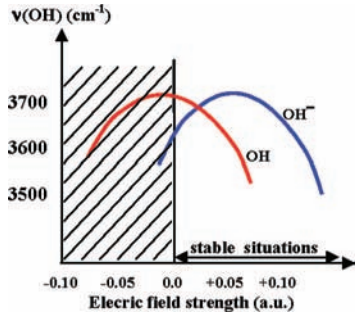

Figure 2. Generic sketch of literature results from ab initio calculations for an isolated OH^- ion and an isolated neutral OH group (e.g., in a water molecule) exposed to an external uniform electrostatic field of varying strength (freely after ref 15). For the electric field, 1 au = 5.14×10^{11} V/m.

and gas-to-solid frequency shifts in good agreement with experiment for both the Raman- and IR-active OH stretching modes.

In the present study, we will calculate *uncoupled isotope-isolated OH frequencies*; i.e., we will make use of the same trick as is often employed in IR and Raman experiments. With this technique, a small fraction of OH groups is dispersed among a large number of OD groups (or vice versa). This facilitates the interpretation of the condensed-phase spectra, because it removes most of the couplings between the hydroxide groups. Additionally, it facilitates the calculations, because we do not need to carry out any 2-D vibrational analysis. The fundamental frequency of the isotope-isolated OH mode in the $Li(OH)_{0.05}(OD)_{0.95}$ crystal is 3670 cm^{-1} (IR measurements in ref 7 by Buchanan et al.); i.e., it is upshifted by +114 cm^{-1} with respect to the frequency of the gas-phase hydroxide ion.

The calculated OH vibrational frequency for the LiOH crystal and for subsystems taken out of the crystal will be presented and discussed together with the features of the electron density and the electronic band structure. We will show how these properties develop as the crystal is built up via its various intra- and interlayer interactions. Finally, we will present a frequency-structure correlation pattern and discuss the origin of the OH frequency upshift for the LiOH crystal.

Figure 2 will be of assistance in our analysis. This figure is the synopsis of several published ab initio studies for the isolated OH^- ion and the water molecule in uniform and nonuniform electric fields of varying strengths (see, for example, refs 12−15 for the OH^- ion and refs 15 and 16 for the water molecule). The figure shows that the frequency of an isolated OH^- ion varies in a parabola-like manner when exposed to uniform electric fields of different strengths. The interaction between the external electric field and the OH^- ion gives rise to an energy contribution which depends on the electric field component along the OH bond, $E_{||}$, and the derivative of the permanent and induced dipole moments with respect to the stretching coordinate, i.e., $E_{||} \cdot d\mu^0/dr_{OH}$ and $E_{||} \cdot d\mu^{ind}/dr_{OH}$. The result is a parabola-like curve as a function of the electric field strength, and because $d\mu^0/dr_{OH}$ and $d\mu^{ind}/dr_{OH}$ have different signs for the hydroxide ion, the maximum frequency occurs at a positive field value.[12–15]

The layout of the paper is as follows. The potential energy curves are calculated within the framework of plane-wave DFT calculations as discussed in section 2 (Method). Section 3 presents the results: the nature of the OH group (section 3.1), the OH vibrational frequencies (section 3.2) and features of the interlayer O−H - - - H−O interaction (section 3.3). Conclusions are given in section 4.

TABLE 1: LiOH Structure from DFT Calculations (This Work) and from Experiment (X-ray Diffraction[3,4] and Neutron Diffraction[5])[a]

	DFT-optimized structure	diffraction
space group	*P4/nmm* (ref 3)	*P4/nmm* (ref 3)
cell vol (Å^3)	52.35	54.59 (ref 4)
a (Å)	3.419	3.549 (ref 4)
c (Å)	4.479	4.334 (ref 4)
z_O	0.1872	0.1938(4) (ref 5)
z_H	0.4042	0.410(1) (ref 5)
$r(O_A-H_A)$ (Å)	0.9720	0.937
$R(O_A-Li_A)$ (Å)	1.904	1.963
$R(O_A-O_B)$ (Å)	2.946	3.020
$R(O_A-O_A)$ (Å)	3.419	3.549
$R(O_A-O_B')$ (Å)	3.701	3.653
$R(O_A-O_A')$ (Å)	4.479	4.334
$R(H_A-H_B')$ (Å)	2.565	2.628
$R(H_A-O_B')$ (Å)	3.032	3.041
$R(H_A-Li_B')$ (Å)	3.169	3.112

[a] The fractional coordinates of the atoms in the crystallographic unit cell are (0, 0, 0) and ($^1/_2$, $^1/_2$, 0) for Li, (0, $^1/_2$, z_O) and ($^1/_2$, 0, 1 − z_O) for O, and (0, $^1/_2$, z_H) and ($^1/_2$, 0, 1 − z_H) for H. The labels *A*, *B*, *A′* and *B′* for the distances refer to the atomic layers defined in Figure 1.

2. Method

2.1. System Descriptions.

The LiOH Crystal and the Isolated Slab. In ref 11 the LiOH crystal structure was optimized using DFT calculations (of the PW91 type, see below) for the crystallographic unit cell within the experimentally determined *P4/nmm* space group, i.e., with two formula units per cell. Structural data for the optimized crystal structure are listed in Table 1, together with the diffraction-determined structure at room temperature.

On the basis of the optimized structure found in ref. 11, we have here performed a series of DFT calculations of the electron density, the electronic band structure, and the intramolecular potential energy curve for *r*(O−H). Various supercells were used for these investigations, depending on the purpose of the calculations. The electron density and the band structure calculations for the crystal were performed for the normal 1 × 1 × 1 crystallographic cell, whereas the vibrational calculations were based on a 2 × 2 × 2 supercell, containing 16 hydroxide ions and 16 lithium ions. This supercell corresponds to a $Li(OH)_{0.065}(OD)_{0.935}$ crystal, and allows one OH^- ion in the supercell to vibrate in a decoupled fashion among 15 OD^- ions and the lithium ions. Experimental results are available for the $Li(OH)_{0.05}(OD)_{0.95}$ crystal.[7]

Calculations were also performed for "contracted" and "elongated" LiOH crystals, where the O−H - - - H−O interlayer distance was varied by changing the *c*-axis stepwise from 3.479 to 16.479 Å, while the *a* and *b* axes and the atomic positions within the layers were kept fixed at the equilibrium values. The results are used in the discussion of the dependence of the OH frequency on the influence from the "opposite" layer in the crystal. The system with the largest *c* axis will be referred to as *the isolated slab* or *the isolated layer.* The interlayer interaction was found to be negligible for *c* larger than approximately 8 Å.

Crystalline Cluster Fragments and the Isolated Ion and Radical. Calculations were performed for the neutral $OH^\cdot$ radical, the isolated OH^- ion, and $(Li^+)_nOH^-$ (with n = 1, 2, 3, 4) crystalline fragment clusters taken from the optimized crystal structure and kept at that geometry. In each case, the molecule/ion/cluster was placed in a cubic box with side length equal to 13 Å.

2.2. Computational Details. The calculations were performed as in ref. 11, i.e., with the Vienna Ab initio Simulation Package (VASP)[17−19] and the PW91[20] GGA functional for exchange and correlation, together with ultrasoft pseudopotentials (US-PP).[21,22] The O 1s and Li 1s electrons were treated as core electrons, and for the valence electrons, the standard "O" and "Li" and "H" US-PPs of the VASP program were used. The energy cutoff was 495 eV (the high-precision, PREC = High, flag was set). The SCF electronic convergence threshold was set to 0.01 meV/cell. An $11 \times 11 \times 11$ k-point mesh, determined by the Monkhorst−Pack scheme, was used for the normal crystallographic cell as well as for the contracted and expanded cells, a $4 \times 4 \times 4$ mesh was used for the $2 \times 2 \times 2$ supercell, and a $4 \times 4 \times 4$ mesh for the cluster calculations. For the systems with an odd number of electrons, the calculations were spin-polarized.

2.3. Calculation of OH Vibrational Frequencies. The vibrational OH frequencies calculated all correspond to the uncoupled vibration of one OH group around its center of mass, keeping all other O, H and Li atoms fixed. Such a mode is a good model for the proper normal mode for the isotope-isolated $Li(OH)_x(OD)_{1-x}$ crystal. That this is so can be deduced from the IR measurements for $Li(OH)_{0.05}(OD)_{0.95}$ and $Li(OD)_{0.05}(OH)_{0.95}$ crystals by Buchanan et al.[7] These measurements gave a $\nu(OH)/\nu(OD)$ of 1.356, which is close to the ratio obtained experimentally for the gas-phase hydroxide ions, namely 1.354.[2,23] Thus, for theoretical calculations of the OH stretching vibrational frequency of an isotope-isolated $Li(OH)_x(OD)_{1-x}$ crystal, the 1-D anharmonic model is quite appropriate.

All frequency calculations were based on potential energy curves generated from single-point plane-wave DFT calculations. We essentially followed the one-dimensional anharmonic procedure as coded by Wójcik et al.[24] Thus, in the case of the various crystal systems (normal, or with expanded or contracted c axis), one OH group in the $2 \times 2 \times 2$ supercell was stretched and contracted around its center of mass, while all other atoms in the supercell were kept fixed at their optimized positions. The step-length was 0.015 Å and some 15 energy points were calculated along the potential energy curve. A polynomial $V(q) = V_0 + \Sigma k_n \cdot \Delta q^n$ ($n = 1,..., 0.7$) was fitted to the potential curve, giving the force constants and the minimum-energy value, r_e. A one-dimensional vibrational Schrödinger equation, defined as $H = -\hbar^2/2M) \cdot [\partial^2/\partial q^2] + V(q)$, with $q = \Delta r_{OH}$ and $M = (m_H \cdot m_O)/(m_H + m_O) = 0.9481$ amu, was solved variationally using 15 harmonic oscillator functions as basis functions. The energy difference between the ground level and the first excited level gives the 1-D anharmonic vibrational frequency reported in this paper. The harmonic frequency was calculated from the second-order force constants obtained from the polynomial fit.

An equivalent procedure was used for all the systems in this paper, i.e., also for the crystal cluster fragments and the isolated OH^- ion.

2.4. Calculation of the External Electric Field. It would be very informative to partition the total electric field (at an arbitrary point within the OH group in the LiOH crystal) into a contribution arising from the *neighbors* outside the OH group (we will call this "the external electric field") and a contribution arising from *within* the molecule itself. Unfortunately, there is no perfect way to achieve this.

For example, to obtain the "external" (or intermolecular) electric field, we *cannot* just compute the total field at, say, the H position in the LiOH crystal, and then subtract the "internal part of the electric field" taken from *the isolated hydroxide ion*, because the ion itself becomes polarized by the crystal and this changes the internal part of the field at H. In the present paper, we have calculated an *estimate of the external electric field at H* by removing one OH^- ion from the system and then calculated the wave function for the remaining system and the electric field at the equilibrium position of the (removed) H. To avoid unwanted vacancy−vacancy interactions, we used a $3 \times 3 \times 2$ supercell for the electric field calculations for the crystal and the isolated layer. For the clusters, the electric field was calculated in an equivalent way, but here the systems were treated as truly isolated systems without periodicity.

All the electric field calculations were performed with the CRYSTAL03 program[25] (with the PW91 functional and local basis-sets from ref 26, i.e., of triple-ζ quality for O and double-ζ quality for Li and H), because we did not manage to make the plane-wave calculations converge for all of the systems studied in this paper. In this paper we will use the electric field for qualitative discussions and do not depend on very exact field values. However, it is perhaps comforting to know that, for the LiOH crystal at equilibrium, where both CRYSTAL03 and VASP calculations worked well for us, the external electric field at H came out to be 0.054 and 0.055 au, respectively.

We define the electric field over an OH group as *positive* along the molecular axis if it is oriented as if there were positive charges on the oxygen side of the molecule and negative charges on the H side, i.e.,

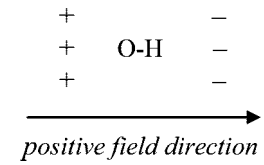

This is "the natural", stable field direction for a real system at equilibrium. In the LiOH crystal, and in other real systems, the field is of course nonuniform.

3. Results and Discussion

3.1. Nature of the OH Group. Here we will first establish the nature of the OH group in LiOH(s). The charge distribution in LiOH(s) was studied already over forty years ago, when Campbell and Coogan[27] used a point-charge model to calculate the lattice energy, the electric field gradient at the nuclei, and the ^{7}Li quadrupole coupling constant, and compared with existing experimental data. They concluded that both H and O are negatively charged. Thirty years ago, Göttlicher and Kieselbach determined the electron density distribution in LiOH from X-ray diffraction,[4] integrated it, and reported the net atomic charges to be $Li^{+1}O^{-0.7}H^{-0.3}$. Soon after, in a combined X-ray and neutron diffraction study, Mair[5] analyzed the electron density in the LiOH crystal and compared it to a quantum-mechanically calculated electron density map for an isolated OH^- ion, which had been exposed to thermal smearing. The agreement was qualitatively very good and she ascribed the remaining differences to intermolecular interactions (polarization effects from the surrounding ions). The recent local basis-set B3LYP calculations by Mérawa et al.,[10] gave Mulliken charges of −1.251, +0.315 and +0.936, for O, H and Li, respectively, i.e., a net charge of −0.95 for the OH group.

From our calculated wavefunction for the crystal we have calculated atomic charges using Richard Bader's Atoms in Molecules theory.[28] However, a Li pseudopotential with only one valence electron was used in the VASP calculations, and the density around the lithium atom was found to be too small

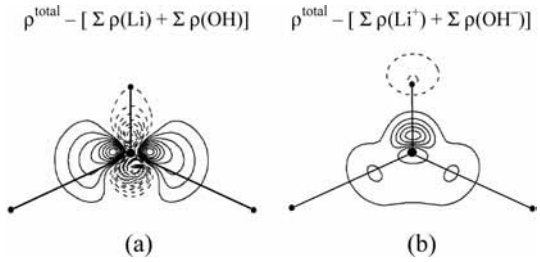

Figure 3. DFT-calculated difference electron density for the optimized LiOH crystal, shown in the Li−OH−Li plane. Contour interval: ±0.05 e/Å^3. Solid lines indicate electron excess, dashed line electron loss; the zero contour is omitted. (a) $\Delta\rho(\mathbf{r}) = \rho^{\text{crystal}}(\mathbf{r}) - \Sigma[\rho(\text{Li}) + \rho(\text{OH}^\bullet)]$, where the sum is taken over all "molecules" in the crystal. (b) $\Delta\rho(\mathbf{r}) = \rho^{\text{crystal}}(\mathbf{r}) - \Sigma[\rho(\text{Li}^+) + \rho(\text{OH}^-)]$, where the sum is taken over all "molecules" in the crystal.

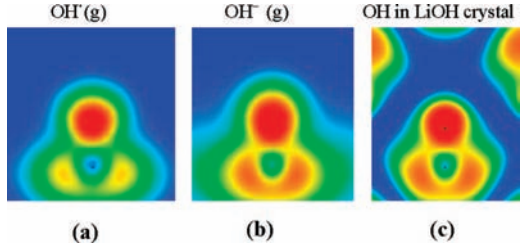

Figure 4. DFT-calculated ELF plots: (a) through an isolated OH radical; (b) through an isolated OH$^-$ ion; (c) in the Li−OH−Li plane of the LiOH crystal.

to locate critical points between lithium and the other atoms. This fact can be seen as an indirect proof that the lithium charge in this crystal is close to +1.

The difference electron density for the LiOH crystal was calculated using *either* the free OH$^-$ ion (and Li$^+$) *or* the free OH$^\bullet$ radical (and Li$^\bullet$) as the reference states (Figure 3). The map with neutral reference molecules is seen to contain significantly more pronounced features than when OH$^-$ is the reference state, in agreement with the notion that the OH group in LiOH(s) is close to being OH$^-$. We have also calculated the electron localization function (ELF)[29] for the crystal and for the isolated OH$^-$ ion and OH$^\bullet$ molecule. The ELF features of the OH group in the crystal are clearly more similar to an OH$^-$ ion than an OH$^\bullet$ group (Figure 4).

We conclude that the OH group in the LiOH crystal is very much like a (polarized) OH$^-$ ion.

3.2. OH Vibrational Shift in LiOH: The Reason for the Upshift. The calculated uncoupled anharmonic OH stretching vibrational frequency for the LiOH crystal is given in the last row in Table 2. The upshift with respect to the isolated ion is +102 cm^{-1}, in quite good agreement with the experimental gas-to-solid shift of +114 cm^{-1}. For both the isolated ion and the crystal, the calculated absolute frequency lies 60−70 cm^{-1} below the respective experimental value and we ascribe this discrepancy to systematic errors in the DFT (i.e., PW91/US-PP) description of the electronic structure.[11]

The external electric field component along the OH bond, $E_{||}$, exerted on the H atom by all the OH$^-$ ion's neighbors in the crystal is listed in the last column in Table 2, and it is seen to be appreciable (0.0535 au). This is the key to the observed OH frequency shift in LiOH. Figure 2 *predicts* that, for bonding situations dominated by electrostatic interaction, an upshift will be observed when the OH$^-$ ion resides in a medium-strong positive electric field, and a downshift when it resides in a very strong positive field. But does Figure 2 have any bearing on the frequency vs field correlations for the LiOH crystal? We shall study Table 2 for guidance.

Going down Table 2 from the first row to the last, we can follow how ν(OH) develops as the crystal is built up "from small to large", i.e., from *the isolated OH$^-$ ion → OH$^-$ with its nearest neighbors → the infinite LiOH layer → the LiOH crystal.*

At first glance, the frequency variation as a function of system size appears rather unsystematic. However, if we plot all these OH frequencies against $E_{||}$, we obtain a much more systematic variation, namely a parabola-like variation (Figure 5). The OH$^-$ ion in the LiOH crystal and its subsystems thus displays a frequency variation that is qualitatively similar to that in Figure 2. This is interesting, and consistent with our expectations that the hydroxide ion behaves in a qualitatively similar way in different environments dominated by electrostatic interactions,[12−15] although electric field inhomogeneity and electronic overlap effects will modify the details of the frequency-field correlation in each particular case. The point corresponding to the LiOH crystal is found close to the top of the parabola, slightly south-southeast of the point for the isolated layer. We conclude that we can explain the experimentally observed frequency upshift for the LiOH crystal largely on electrostatic grounds, and that the upshift originates from the interactions present *within* the isolated LiOH layer (whereas the *interlayer* interactions induce a frequency downshift).

TABLE 2: Intramolecular OH Vibrational Frequency and Bond Length for the OH$^-$ Ion in the Optimized LiOH Crystal and in Various Subsystems Taken out of This Crystal (and Kept at the Same Geometry, except for the *r*(OH) Distance)[a]

system	ν	$\Delta\nu$	ω	$\Delta\omega$	r_e(OH)	Δr_e(OH)	$E_{\|\|}$ (au)
OH^{-b}	3496	0	3702	0	0.9785	0	0
$(Li^+)_nOH^-$							
$n = 1$	3588	+ 92	3788	+ 86	0.9736	−0.0049	0.3285
$n = 2$[c]	3606	+110	3804	+102	0.9729	−0.0058	0.0660
$n = 2$[d]	3582	+ 86	3767	+ 65	0.9755	−0.0030	0.0655
$n = 3$	3511	+ 15	3713	+ 11	0.9797	+0.0012	0.0980
$n = 4$	3366	−130	3577	−125	0.9892	+0.0107	0.1303
LiOH layer	3653	+157	3839	+137	0.9696	−0.0091	0.0487
LiOH crystal[e]	3598	+102	3787	+85	0.9720	−0.0107	0.0535

[a] The quantities listed are the isotope-isolated anharmonic (ν) and harmonic (ω) OH vibrational frequencies, the intramolecular equilibrium distance (r_e(OH)) and the parallel component of the external electric field at the H atom ($E_{||}$; defined in section 2.4). The frequency shifts ($\Delta\nu$ and $\Delta\omega$) and the distance shift (Δr_e) are given with respect to the optimized isolated OH$^-$ ion. Electronic structure calculations at the DFT level. (0.01 au for the electric field = 5.14 × 10^6 V/cm). [b] The experimental values for the isolated OH$^-$ ion are 3555.606 cm^{-1}, 3738.4 cm^{-1} and 0.96431 Å for ν, ω and r_e(OH), respectively, as derived from velocity modulation laser spectroscopic measurements in the infrared region.[2] [c] C_{2v} symmetry. [d] C_s symmetry. [e] The experimental frequency ν for the isotope-isolated LiOH crystal is 3670 cm^{-1} and the gas-to-crystal frequency shift $\Delta\nu$ is +114 cm^{-1}.[7] The experimental r_e(OH) value for the crystal is 0.937 Å.

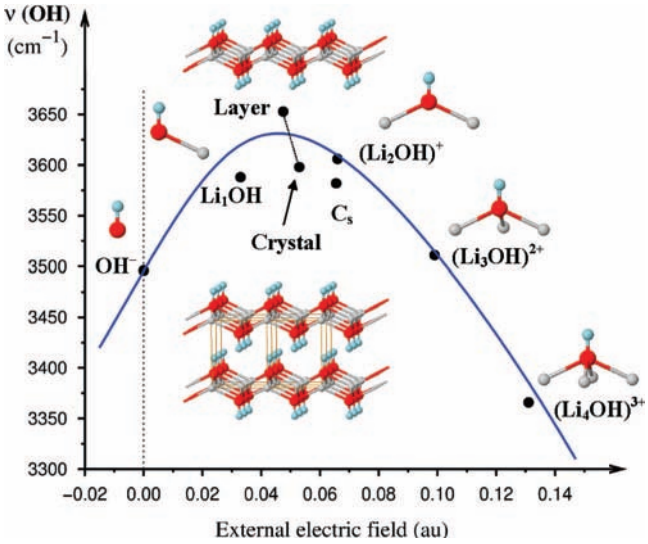

Figure 5. DFT-calculated anharmonic uncoupled OH stretching vibrational frequency (in cm^{-1}) in the LiOH crystal and in various fragments taken out of the crystal, plotted as a function of the parallel component of the external electric field at the hydroxide ion's H position (see text). The curve has been drawn as a guide to the eye. The line running downward from the isolated-layer point to the optimized-crystal point originates from a series of calculations with an expanded *c* axis.

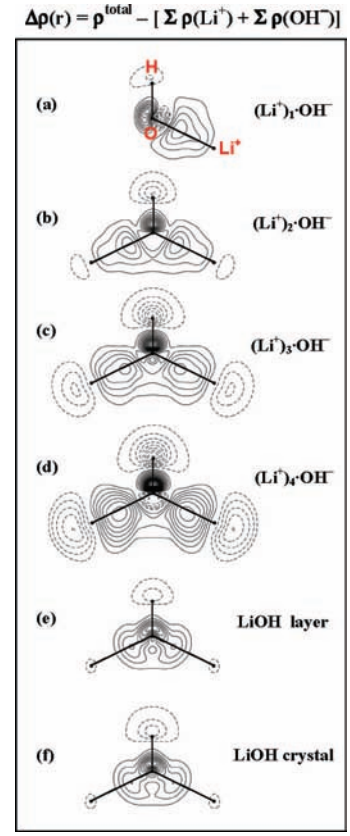

Figure 6. DFT-calculated difference electron density, $\Delta\rho(\mathbf{r}) = \rho^{\text{total}} - \Sigma[\rho(\text{Li}^+) + \rho(\text{OH}^-)]$, for the optimized LiOH crystal as well as for the $(\text{Li}^+)_n(\text{OH}^-)$ clusters (n = 1, 2, 3, 4) and the isolated LiOH layer "taken out of the crystal". In all cases the geometry for the optimized LiOH crystal is used. The section shown lies in the Li−OH−Li plane. Contour interval: ±0.05 e/Å^3. Solid lines indicate electron excess; dashed line, electron loss. The zero contour is omitted.

It is instructive to discuss the OH frequency and the electron density variations together. The difference electron density with respect to the constituent ions, i.e., $\Delta\rho = \rho^{\text{tot}}(\mathbf{r}) - [\Sigma\rho(\text{Li}^+) + \Sigma\rho(\text{OH}^-)]$, shows how the OH$^-$ ion becomes more polarized as more cation neighbors are added (Figure 6a−d), and the external field over the ion increases. At the same time, the OH frequency first goes up and then down as we follow the parabola "toward the right" in Figure 5. The change of environmental influence occurring between the isolated $(\text{Li}^+)_4\text{OH}^-$ cluster and the infinite LiOH layer is also drastic: the electric field at H is seen to diminish to less than half when the rest of the layer is added. This reduction of the field *affects the electron density* such that it pushes some electron density back to H (Figure 6e), and it *affects the frequency* such that we should follow the parabola "toward the left" in Figure 5; the results is a large OH frequency upshift. The DFT-calculated OH frequency of the LiOH layer lies as much as +320 cm^{-1} above the $(\text{Li}^+)_4\text{OH}^-$ frequency.

Going from the isolated slab to the full LiOH crystal, the neighbors in the opposite layer (and all other layers) are added. The effects on the electron density map from this addition are modest (Figure 6f). For the frequency, we follow the line from ″Layer″ to ″Crystal″ in Figure 5 downward; the downshift is approximately −60 cm^{-1}. (The deviation of this line from the ideal parabola-like curve of the uniform field is likely to be a geometric effect; the nonuniformity of the electrostatic field needs to be taken into account for a more precise frequency vs field correlation treatment in each particular case).

3.3. Interlayer Interaction. The LiOH layers are held together rather weakly in the LiOH crystal. Above, we found a modest OH frequency downshift arising from the interlayer interaction, and our VASP calculations of the total energy variation as a function of the interlayer distance give a minimum (at c = 4.479 Å) which is only 0.07 eV deep.

The *electrostatic potential* in Figure 7 will shed further light on the interlayer interaction. It shows a representative section through the isolated LiOH layer. Let us place a LiOH "probe" layer below the first layer, as illustrated in the right part of the figure. In the section shown, the isolated layer is seen to generate a negative electrostatic potential below it (i.e., it stabilizes the positive Li and H atoms in the layer below but destabilizes the O atoms). The isolated layer thus effectively acts as a net negative neighbor δ^- to the layer below, and the OH groups from the layer below will be involved in $[\text{O}^{\delta-}\text{H}^{\delta+}]^-$ - - - δ^- interactions (in addition to any nonelectrostatic interactions). The presence of a $[\text{O}^{\delta-}\text{H}^{\delta+}]^-$ - - - δ^- arrangement neither supports nor excludes the possibility that the layers are hydrogen-bonded, because hydrogen-bonding is to a large degree electrostatic in nature. However, the staggered O−H - - - H−O geometries found here, and in many other layered minerals, are particularly unfavorable for H-bonding. Thus these antiparallel negative OH ions are not hydrogen-bonded. (Incidentally, a Bader-type topology analysis[28] of the electron density gives no H - - - O bond critical points).

The potential energy contour map also shows that the slope of the electrostatic potential generated by the upper layer at the position of the H atoms in the lower layer in Figure 7 is negative, i.e., *the electric field* "from the opposite layer" is positive at the H position of the OH groups in the layer below, in agreement with our explicit calculations of the electric field outside an isolated slab, as presented in Table 2 and Figure 5.

The variations of the O−H vibrational frequency and of the *electric field generated by the opposite layer* as the layers are brought closer and closer together are shown in Figure 8. We see that, except for the sharp frequency upshift

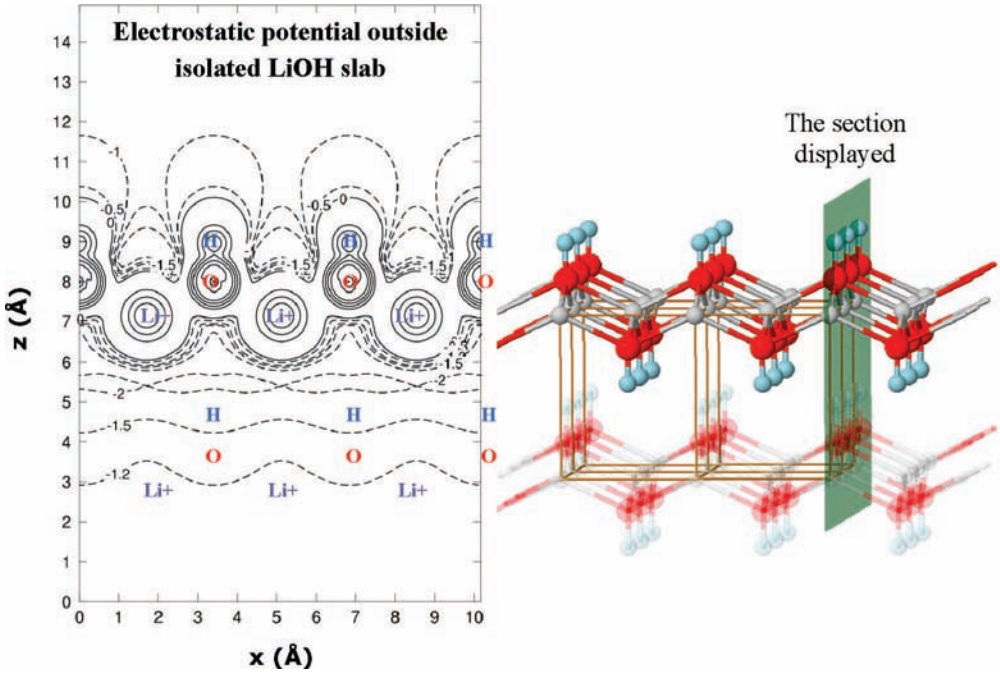

Figure 7. Electrostatic potential outside an isolated LiOH slab. The atomic labels below the layer refer to the probe sites, which are located exactly at the positions of the layer below in the LiOH crystals. The probe layer has been blurred in the picture to the right.

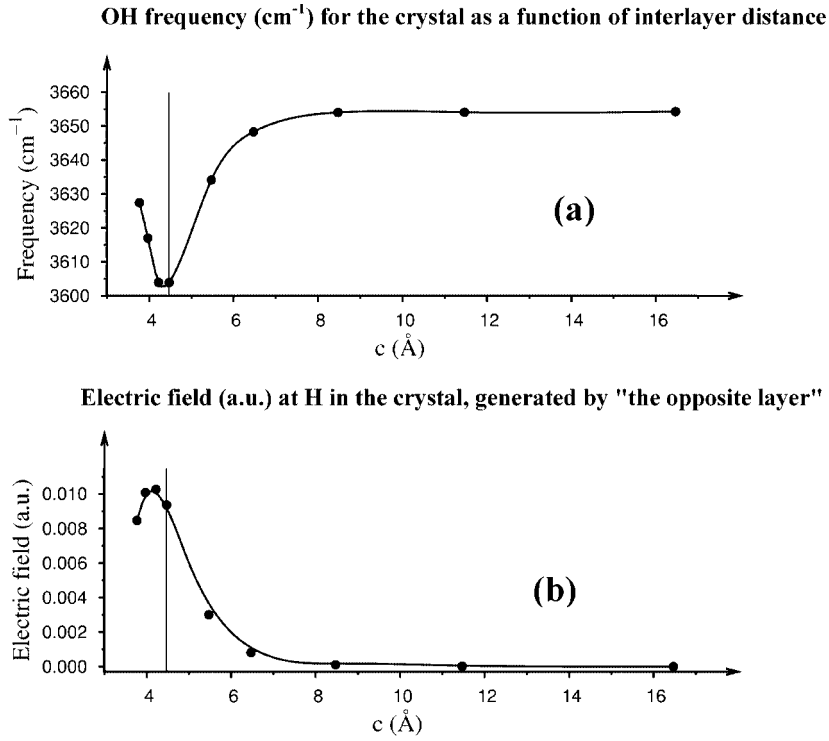

Figure 8. DFT-calculated anharmonic OH frequency plotted as a function of the interlayer separation in the LiOH crystal, expressed as the length of the *c* cell axis. For each value of the c parameter, the external electric field at the "equivalent position" outside an isolated slab was calculated, i.e., at the position corresponding to the equilibrium position of the vibrating H in the crystalline system.

occurring when the *c* parameter is pushed well below the equilibrium value, there is a one-to-one correlation between the frequency and the electric field. This is yet another demonstration of the key role played by the elecrostatic interactions in determining the OH vibrational frequency in the LiOH system. The large upshift for the short interlayer distance should largely be a consequence of exchange repulsion interactions.

Although electrostatic interactions are important in the ionic LiOH crystal, nonelectrostatic interactions of course also play a role. The dispersion in *electronic band structure* for the LiOH crystal (Figure 9a) bears witness of that. The valence band ("O *lp*") has O $2p_x$ and $2p_y$ lone-pair character, and the band in the region around −4 eV consists mainly of O $2p_z$ and H 1s contributions and corresponds to the covalent σ orbitals within the OH^- ions. The band structure for a

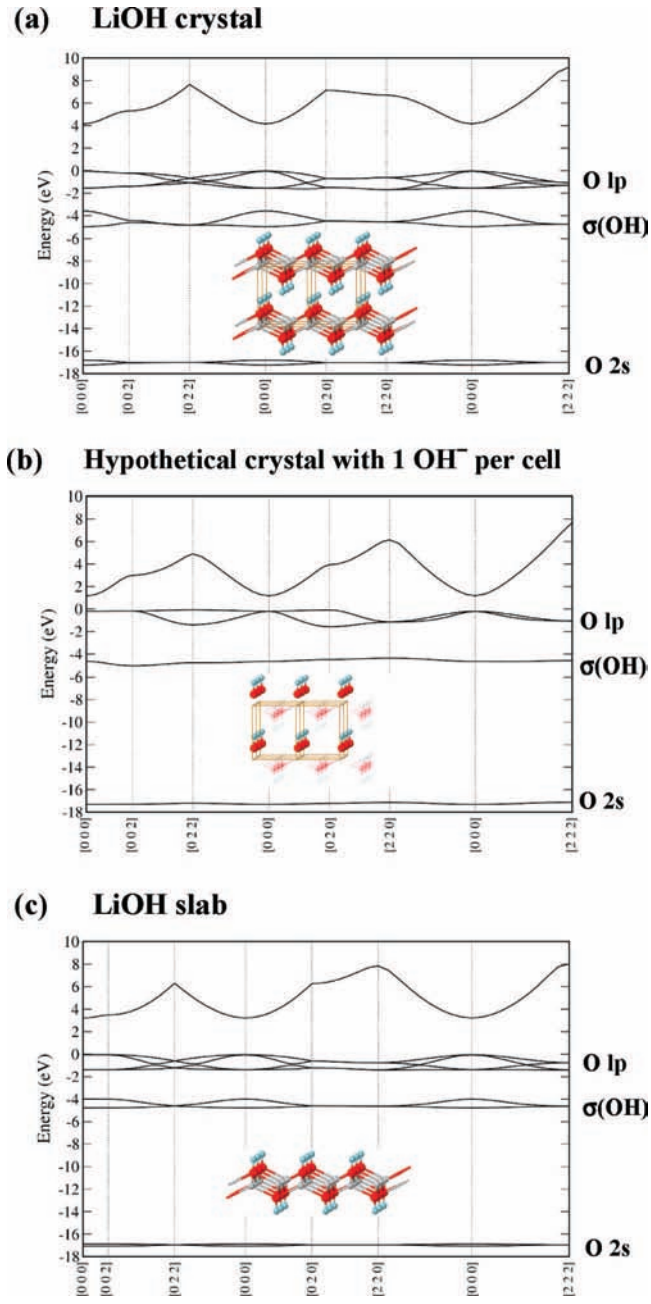

Figure 9. DFT-calculated electronic band structure for the three systems shown in the figure, all with the geometry of the optimized LiOH crystal: (a) the LiOH crystal; (b) a hypothetical structure with a single OH^- anion in the unit cell; (c) the isolated LiOH slab. The top of the valence band is at $E = 0.0$ eV. The wavevector $[k_x, k_y, k_z]$ is given in units of the reciprocal cell lengths times 4.

hypothetical crystal containing one OH^- ion (and nothing else) in a unit cell of the same dimensions as LiOH is given in Figure 9b. A comparison between Figure 9a and Figure 9b shows that the dispersion of the O *lp* band in the LiOH crystal is almost entirely due to orbital overlap between parallel OH^- ions within the same LiOH layer. A comparison between Figure 9a and the band structure for the LiOH slab in Figure 9c shows that the dispersion of the σ(OH) band is partly due to interlayer electronic overlap.

4. Summary and Concluding Remarks

The specific goal of the present article was to explain why the OH frequency is upshifted in some crystalline hydroxides such as LiOH; i.e., we wanted to find the structural features which lead to the OH^- vibrational upshift. Here we have found that it is the intralayer (electrostatic and polarization) interactions, i.e., the cation and anion neighbours on the O side of the OH^- ion, which are the key reason behind the large upshift observed in the LiOH crystal. More precisely we have found that:

(i) The observed OH^- upshift in the LiOH(s) crystal is the *net result* of a number of strong positive and negative-field interactions within the layer and a weaker one between the layers. Thus the hydroxide ion's four nearest Li^+ neighbors give rise to a frequency downshift of -125 cm^{-1}, then the rest of the layer contributes with an upshift of $\sim+275$ cm^{-1}, and finally, the interlayer interaction in the crystal gives a downshifting contribution of ~-60 cm^{-1}. The net effect of all this is a frequency upshift of $\sim+100$ cm^{-1}.

(ii) The interlayer interactions, including the O−H - - - H−O interactions, are largely electrostatic in character. No H-bonds are present.

(iii) The OH frequency shifts calculated here for the LiOH(s) crystal and for several subsystems taken out of the crystal can be systematized using the electric field strength (exerted on the OH^- ion by its neighbors) as a variable. The curve has a parabola-like shape. The electric field strength for the full crystal is of moderate magnitude and therefore falls close to the maximum of the parabola. This qualitatively explains why the OH frequency in the crystal shows a large gas-to-solid upshift (both in experiment and in calculations). The underlying reason for the frequency upshift in the crystal is the negative sign of the hydroxide ion's permanent dipole moment derivative, $d\mu^0/dq$, along the stretching coordinate.[15]

Acknowledgment. Financial support from the Swedish Research Council (VR) and the EU project HPRN-CT-2000-19 are gratefully acknowledged. Useful discussions with Drs. Anders Eriksson Uppsala University) and Henrik Skogby (Naturhistoriska Riksmuseet) are also gratefully acknowledged.

References and Notes

(1) W, S; Benedict, N.; Gailar, E. K.; Plyler, J. *Chem. Phys.* **1956**, *24*, 1139.
(2) Owrutsky, J. C.; Rosenbaum, N. H.; Tack, L. M; Saykally, R. J. *J. Chem. Phys.* **1985**, *83*, 5338.
(3) Ernst, Th. *Z. Phys. Chem* **1933**, *B20*, 65.
(4) Göttlicher, S.; Kieselbach, B. *Acta Crystallogr.* **1976**, *A32*, 185.
(5) Mair, S. L. *Acta Crystallogr.* **1978**, *A34*, 542.
(6) Hase, Y.; Yoshida, I. V. P. *Chem. Phys. Lett.* **1979**, *65*, 46.
(7) Buchanan, R. A.; Kinsey, E. L.; Caspers, H. H. *J. Chem. Phys.* **1962**, *36*, 2665.
(8) Yoshida, I. V. P.; Hase, Y. *Spectrotrosc. Lett.* **1979**, *12*, 409.
(9) Tanigawa, H.; Tanaka, S. *J. Nucl. Sci. Technol.* **2001**, *38*, 1005.
(10) Mérawa, M.; Labequerie, P.; Ugliengo, P.; Doll, K.; Dovesi, R. *Chem. Phys. Lett.* **2004**, *387*, 453.
(11) Gajewski, G.; Mitev, P.; Hermansson, K. *J. Chem. Phys.* **2008**, *129*, 064502.
(12) Hermansson, K. *J. Chem. Phys.* **1991**, *95*, 3578.
(13) Hermansson, K. *Chem. Phys.* **1992**, *159*, 67.
(14) Hermansson, K. *Chem. Phys.* **1993**, *170*, 177.
(15) Hermansson, K. *Int. J. Quantum Chem.* **1993**, *45*, 747; Eratum. *Int. J. Quantum Chem.* **1993**, *47*, 175.
(16) Hermansson, K. *J. Chem. Phys.* **1993**, *99*, 861.
(17) Kresse, G.; Hafner, J. *Phys. Rev. B* **1993**, *47*, 558; *Phys. Rev. B* **1994**, *49*, 14251.
(18) Kresse, G.; Furthmüller, J. *Phys. Rev. B* **1996**, *54*, 11169.
(19) Kresse, G.; Furthmüller, J. *Comput. Mater. Sci.* **1996**, *6*, 15.
(20) Perdew, J. P.; Chevary, J. A.; Vosko, S. H.; Jackson, K. A.; Pederson, M. R.; Singh, D. J.; Fiolhais, C. *Phys. Rev. B* **1992**, *46*, 6671; *Phys. Rev. B* **1993**, *48*, 4978.
(21) Vanderbilt, D. *Phys. Rev. B* **1990**, *41*, 7892.
(22) Kresse, G.; Hafner, J. *J. Phys.: Condens. Matter* **1994**, *6*, 8245.

(23) Rehfuss, B. D.; Crofton, M. W.; Oka, T. *J. Chem. Phys.* **1986**, *85*, 1785.
(24) Wójcik, M. J.; Lindgren, J.; Tegenfeldt, J. *Chem. Phys. Lett.* **1983**, *99*, 112.
(25) Saunders, V. R.; Dovesi, R.; Roetti, C.; Orlando, R.; Zicovich-Wilson, C. M.; Harrison, N. M.; Doll, K.; Civalleri, B.; Bush, I.; D'Arco, Ph.; Llunell, M. *CRYSTAL2003 User's Manual*; University of Torino: Torino, 2003.
(26) Ojamäe, L.; Hermansson, K.; Pisani, C.; Causà, M.; Roetti, C. *Acta Crystallogr.* **1994**, *B50*, 268.
(27) Campbell, I. D.; Coogan, C. K. *J. Chem. Phys.* **1965**, *42*, 2738.
(28) Bader, R. F. W. *Atoms in Molecules - A Quantum Theory*; Oxford University Press: Oxford, U.K., 1990.
(29) Becke, A. D.; Edgecombe, K. E. *J. Chem. Phys.* **1990**, *92*, 5397.

JP802426D